



# Synthesis, characterization and photocatalytic activity of a composite based on TiO<sub>2</sub> and active carbon prepared from mango pit

Síntese, caracterização e atividade fotocatalítica de um compósito à base TiO<sub>2</sub> e carbono ativo preparado a partir do caroço de manga

L. T. dos S. Ramos<sup>1</sup>; L. M. Santos<sup>2\*</sup>; A. E. H. Machado<sup>3</sup>; M. O. G. Souza<sup>4</sup>

<sup>1</sup>Instituto Federal de Educação, Ciência e Tecnologia Baiano, 48110-000, Catu- Bahia, Brazil

<sup>2</sup>Instituto Federal de Educação, Ciência e Tecnologia de Goiás, 76400-000 Uruaçu-Goiás, Brazil

<sup>3</sup>Instituto de Química/Laboratório de Fotoquímica e Ciências de Materiais, Universidade Federal de Uberlândia, 38400-462, Uberlândia-Minas Gerais, Brazil

<sup>4</sup>Departamento de Ciências Exatas e da Terra, Universidade do Estado da Bahia-Campus I, 41200-105, Salvador-Bahia, Brazil

\*[lidiane.santos@ifg.edu.br](mailto:lidiane.santos@ifg.edu.br)

(Recebido em 16 de janeiro de 2021; aceito em 17 de julho de 2021)

In this study, results are presented concerning the development of alternative materials based on titanium dioxide (TiO<sub>2</sub>) and agro-industrial waste for use in the treatment of effluent contaminated with dyes. The photocatalytic activity of a composite formed by the association of activated carbon, obtained from pit residue of mango, with modified titanium dioxide was evaluated by the degradation of crystal violet dye. From the analysis of X-rays diffratograms, it was observed that the modification introduced in the TiO<sub>2</sub>, as well as the formation of the composite with activated carbon, lead to wider peaks with lesser intensity, suggesting the formation of small particles. The composite presented the best photocatalytic performance, attributed to the significantly large specific area of this material when compared to pure TiO<sub>2</sub>, reaching 99% degradation of the organic matter after 60 minutes of reaction time. This is, therefore, a promising material for environmental photocatalysis.

Keywords: mango pit, TiO<sub>2</sub>/activated carbon, photocatalytic activity.

Neste estudo são apresentados os resultados referentes ao desenvolvimento de materiais alternativos à base de dióxido de titânio (TiO<sub>2</sub>) e resíduos agroindustriais para tratamento de efluentes contaminados com corantes. A atividade fotocatalítica do composto formado pela associação do carvão ativado, obtido de resíduo do caroço de manga, com dióxido de titânio modificado foi avaliada pela degradação do corante cristal violeta. A partir da análise dos difratogramas de raios X, observou-se que a modificação introduzida no TiO<sub>2</sub>, assim como a formação do compósito com o carvão ativado, levava a picos mais largos e com menor intensidade, sugerindo a formação de pequenas partículas. O compósito apresentou o melhor desempenho fotocatalítico, atribuído à área específica significativamente grande deste material quando comparado ao TiO<sub>2</sub> puro, atingindo 99% de degradação da matéria orgânica após 60 minutos de reação. Este é, portanto, um material promissor para fotocatalise ambiental.

Palavras-chaves: caroço de manga, TiO<sub>2</sub>/carbono ativado, atividade fotocatalítica.

## 1. INTRODUCTION

Pollution of water resources is a socio-environmental problem of global importance in modern society. Eminently, dyes have a high potential for contamination. Crystal violet (Colour Index 42555), molecular formula C<sub>25</sub>H<sub>30</sub>ClN<sub>3</sub>, is widely used in the industry for dyeing paper, acrylic fibers and leather, identifying bacteria by the Gram staining method, treating burns and skin lesions, and identifying prints digital. It is a cationic dye that has harmful effects on life, causing irritation to the eyes and digestive tract and, in extreme cases, leading to respiratory and renal failure and carcinogenic potential. Furthermore, this dye can cause long-term effects in aquatic environments [1].

In general, the contamination of residual water by dyes, many of them recalcitrant to classic treatments, results in numerous environmental problems, compromising ecosystems [2]. The presence of colored species in water bodies, even in small concentrations, may present harmful

effects to aquatic biota since it hinders the passage of light, compromising photosynthesis and oxygenation of water [1]. Considering the environmental impacts, together with the concerns about human health, the study of effluent treatment alternatives that promote the efficient removal or elimination of dyes becomes a priority [3].

In this context, we emphasize advanced oxidative processes (AOP) based on the action of free radicals and other active species on organic matter, leading to degradation or even complete mineralization [4, 5]. A particular case of AOP is a heterogeneous photocatalysis employing primarily titanium dioxide ( $\text{TiO}_2$ ) as a catalyst, which has been shown to be effective in the degradation of dyes [6, 7]. However, although thoroughly studied,  $\text{TiO}_2$  presents limitations to large scale applications, such as the need for radiation in the ultraviolet (UV) region for a band gap of 3.2 eV and the rapid recombination of the electron/hole pair beyond the difficulty of separation and regeneration after the process. Thus, it is necessary to develop alternative systems based on  $\text{TiO}_2$  with better photocatalytic properties in relation to commercial oxide, thus increasing the possibility of use in the treatment of effluents [8-10].

Several studies have been published focusing on the development of systems based in the combination of active carbon (or other carbonaceous materials) and semiconductor oxides in order to obtain more active catalysts for different applications [11-13]. Among the different solids, it is important to highlight those obtained from the association between semiconductor and activated carbon nanomaterials, which have advantages such as high specific surface area and the adsorption capacity of organic matter, which tends to favor the photocatalytic process, and the ease of regeneration of these materials [14-17].

According to the literature, active carbon can be obtained from agro-industrial waste such as mango [18, 19], one of the most produced fruits in Brazil. Due to the nutritional and sensorial characteristics of the fruit, there is an expressive consumption of mango in the country, both in natura and in the form of pulp for juice, jellies, and sweets. The industrial processing of the fruit generates a large amount of bark and pits that are discarded as waste, generating a substantial environmental problem [20, 21]. This residue, besides being used in the production of coal (adsorbents), presents a potential resource of raw material in the production of biofuel and as a nutritional by-product [20-23].

In the present study, mango pit was used for the preparation of coal,  $\text{TiO}_2$ -carbon composites, being combined directly with titanium dioxide ( $\text{TiO}_2$ -residue) in order to improve the characteristics of the semiconductor in photocatalytic processes.

## 2. MATERIAL AND METHODS

### 2.1 Synthetic route

#### *Preparation of active carbon from mango pit*

Mango pit (obtained from a fruit pulp mill located in the city of Salvador, Bahia, Brazil) were washed with water to remove impurities and fruit residues. Afterwards, they were sun-dried and then in an oven at 70 °C for 24 hours. The residues were cut and the lumps were oven dried for another 24 hours. Afterwards, they were crushed in a knife mill with the powder obtained and separated in an 80 mesh sieve (sample B). This material was mixed with the activating agent  $\text{ZnCl}_2$  and submitted to a thermal treatment at 500 °C under nitrogen atmosphere, producing the activated carbon (AC). The active carbon was then washed with a solution of hydrochloric acid at 70 °C under stirring for 60 minutes and then washed with hot water until pH around 8.0. The material was again oven dried at 80 °C for 8 hours. The sample B, without the activating agent, was heat treated under the same carbonization conditions of the active carbon, producing the sample CB.

### *Modification in commercial titanium dioxide*

Commercial TiO<sub>2</sub> (P25 Degussa), 0.6 g, was dispersed in 29 mL of NaOH (10 mol L<sup>-1</sup>) solution under vigorous stirring. The obtained mixture was transferred to a teflon beaker, which was inserted into a steel reactor and heated in an oven at 130 °C for 3 hours. At room temperature, the resulting white powder was separated from the aqueous phase by centrifugation and washed with distilled water until a pH close to 8.0. After that, 60 mL of a 0.1 mol L<sup>-1</sup> HCl solution was added to the powder and the resulting suspension was stirred for 2 hours. To promote ion exchange, the acid solution was renewed after 1 hour of stirring. The modified titanium dioxide (NT) was washed with distilled water and dried at 70 °C for 12 hours [24].

### *Synthesis of composites TC e TB*

The active carbon (AC) prepared from mango pit was mixed with the modified titanium dioxide (NT) in the 1:1 mass ratio. The mixture was stirred for 12 hours and then suspended in deionized water, being subsequently centrifuged. After removing the liquid, the material was oven dried at 120 °C for 24 hours and reheated at 500 °C for 1 hour under nitrogen flow. The resulting composite was named TC. The same procedure was repeated using the sample B, thus obtaining the TB composite.

## **2.2 Characterization**

### *Infrared with Fourier Transform (FTIR)*

In FTIR analyses, a Perkin Elmer FTIR Spectrum 100S model was used. The pellets were prepared by mixing the samples to be analyzed with potassium bromide (KBr). The spectra were obtained in the region between 4000 and 400 cm<sup>-1</sup> with 4 cm<sup>-1</sup> resolution.

### *X-ray diffraction (XRD)*

The diffractograms were obtained using a Shimadzu XRD6000 equipment with Cu K $\alpha$  radiation ( $\lambda=1.5418 \text{ \AA}$ ). The experiments were conducted at  $2\theta$  intervals between 20 and 80° with a scanning speed of 2° min<sup>-1</sup>.

### *Thermal analysis (TG/DTA)*

TG/DTA curves were obtained using a Shimadzu TA-60 WS equipment at 25-900 °C min<sup>-1</sup> under N<sub>2</sub> atmosphere. Approximately 10 mg of sample per measurement were packed in a platinum crucible.

### *Nitrogen adsorption/desorption isotherms*

Samples were pretreated for 2 hours at 250 °C under vacuum ( $6.6 \times 10^4 \text{ Pa}$ ). The nitrogen adsorption / desorption isotherms at -196 °C were obtained using a Micrometrics ASAP 2020 equipment.

### *Scanning electron microscopy*

The scanning electron microscopy (SEM) analysis was performed using a Tescan Model VEGA 3 LMU. The samples were placed on a carbon fiber covered stub, and then metallized in a Quorum Technologies Model Q150 RES equipment, where the coating was made by deposition of metallic

ions of gold. The micrographs were obtained using an acceleration voltage of 10 kV and a secondary electron detector.

### *Transmission electron microscopy*

The morphology and particle size distribution of the samples was characterized by, by transmission electron microscopy (TEM), using a model JEM1400 microscope.

### *Diffuse reflectance spectroscopy*

The optical properties of the materials were determined by diffuse reflectance spectroscopy. The spectra were obtained at room temperature using a SHIMADZU UV-1201 spectrophotometer using potassium bromide as the reference.

## 2.3 Photocatalytic assays

The photocatalytic assays were performed using a reactor equipped with a cooling system which allows the solution to be kept under irradiation at a temperature of approximately 30 °C. A high pressure mercury vapor lamp (125 W) was used as source of irradiation (Figure 1).

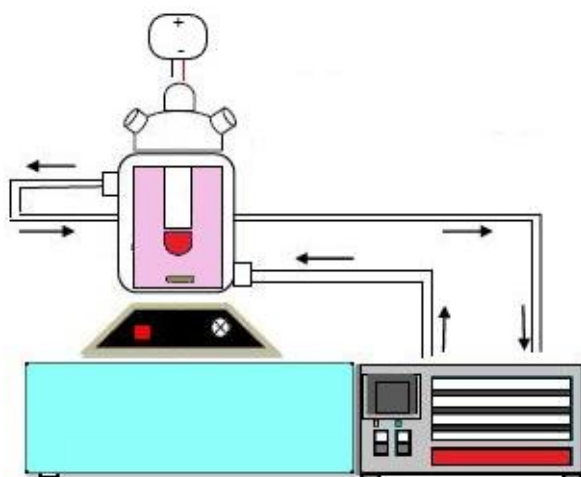


Figure 1: Photocatalytic bench system.

Initially, aiming to evaluate the photodegradation kinetics of crystal violet (CV), dye used as model of oxidizable substrate in the absence of catalyst, its photolysis was carried out by adding only an aqueous solution of the dye (350 mL, 100 mg L<sup>-1</sup>, pH 6.8) to the reactor.

In the photocatalytic assays, 350 mL of the CV solution (100 mg L<sup>-1</sup>, pH 6.8) and 400 mg of the catalyst were added to the reactor. The temperature and pH of the reaction medium was the same as that the previously used. The suspension was stirred in the dark for approximately 15 minutes to establish the adsorption equilibrium between the solution containing the dye and the surface of the catalyst. Then, the mercury vapor lamp was turned on and aliquots were collected at predefined time intervals, centrifuged, being the reaction monitored at 589 nm with the aid of a Perkin Elmer UV-VIS spectrophotometer.

Photocatalytic degradation of the dye was also monitored using measurements of dissolved organic carbon (DOC) using a Shimadzu TOC-VCPH/CPN carbon analyzer equipped with an ASI-V autosampler. The samples were all filtered using 0.45 µm medium porosity filters prior the analysis.

In all experiments, aliquots of 5.0 mL were collected at intervals of 0, 5, 10, 15, 20, 30, 40, 50, and 60 minutes of reaction.

### 3. RESULTS AND DISCUSSION

The infrared spectra of the samples of mango residue before (B) and after heat treatment (CB), and of the activated carbon (AC) are shown in Figure 2.

All samples present wide bands between 3000 and 3500  $\text{cm}^{-1}$  related to stretching frequencies of OH groups at the surface of these materials [11]. In the infrared spectrum of the mango residue (B), absorption bands can be observed at 2922 and 2845  $\text{cm}^{-1}$ . These bands are attributed to methylene (C–H) group vibrations [25]. It can also be observed an absorption band at 1720  $\text{cm}^{-1}$  related to vibrational stretch of carbonyl groups [26], and bands between 1610 and 1500  $\text{cm}^{-1}$  associated to C–C bond in aromatic rings, present in the lignin structure [26]. In addition, a band at 1119  $\text{cm}^{-1}$  can be observed, attributed to C–O–C bonds. When analyzing the spectra of the samples of the thermally treated biomass and the active carbon (CB and AC), the disappearance of some bands is observed, such as for example those observed at 2922  $\text{cm}^{-1}$ , 2845  $\text{cm}^{-1}$ , 1720  $\text{cm}^{-1}$ , and 1119  $\text{cm}^{-1}$  in the biomass spectra. The observed changes in the spectra of these samples are a consequence of the decomposition of the precursors combined with the structural change that occurs during heat treatment [27].

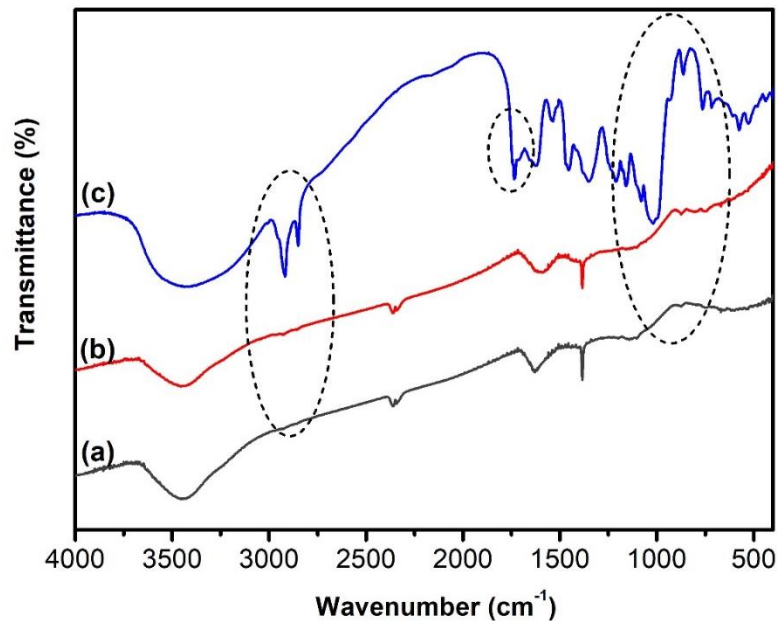


Figure 2: Infrared spectra with Fourier Transform (FTIR) of samples: (a) AC, (b) CB and (c) B.

Infrared spectra (Figure 3) of commercial titanium dioxide ( $\text{TiO}_2$  P25), modified titanium dioxide (NT), and composites (TC and TB) showed similar wide bands between 3000 and 3500  $\text{cm}^{-1}$ . Bands around 1630  $\text{cm}^{-1}$  were also observed, associated to hydroxyl group elongation, indicating the presence of water in the samples [28, 29]. The solids also present a band around 2300  $\text{cm}^{-1}$  and 1380  $\text{cm}^{-1}$ , suggesting C–O and C=O stretching, respectively [30]. The absorption bands around 464  $\text{cm}^{-1}$  and 700  $\text{cm}^{-1}$  can be attributed to Ti–O bonding vibrations, characteristic of Ti–O–Ti [30, 31]. The presence of these bands in TC and TB suggest that the titanium dioxide particles should be covering the surface of the carbonaceous materials in the composites [11].

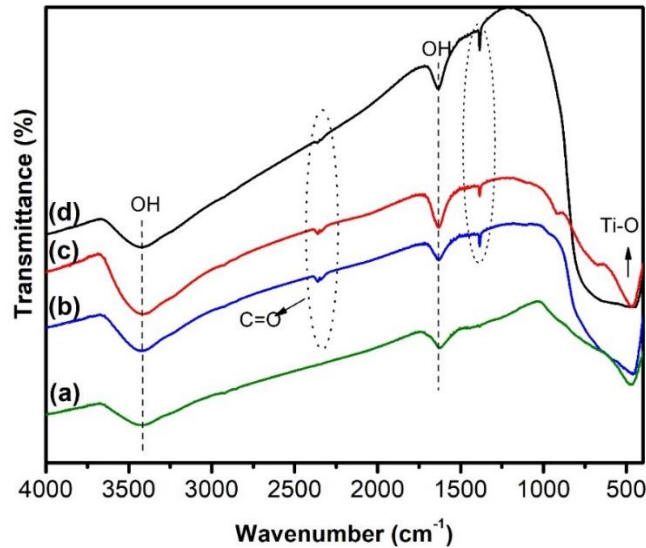


Figure 3: Infrared spectra with Fourier Transform (FTIR) of the photocatalysts: (a) TB - B precursor with modified titanium dioxide (NT), (b) TC - active carbon with modified titanium dioxide (NT), (c) NT - modified TiO<sub>2</sub> P25 and (d) P25 - commercial TiO<sub>2</sub>.

The composition of the phases and the crystallinity of TiO<sub>2</sub> (commercial and modified) and composites were estimated by X-ray diffraction, comparing the results (Figure 4) with references from the JCPDS data bank. In the diffractogram of TiO<sub>2</sub> P25, Bragg reflections at  $2\theta = 25.35^\circ$ ,  $37.83^\circ$ ,  $48.12^\circ$ ,  $54.00^\circ$ ,  $55.15^\circ$ ,  $70.43^\circ$ , and  $75.12^\circ$  were observed, with diffraction planes of (100), (004), (200), (100), (211), (220), and (215), respectively, characteristic of the anatase phase (JCPDS card no. 21-1272). The presence of peaks at  $2\theta = 27.41^\circ$ ,  $36.02^\circ$ ,  $41.22^\circ$ ,  $56.55^\circ$ ,  $62.73^\circ$ , and  $69.01^\circ$  with diffraction planes of (110), (101), (111), (200), (002), and (301), respectively, confirm the presence of the rutile phase (JCPDS card no. 21-1276). Note that the sample presents high crystallinity.

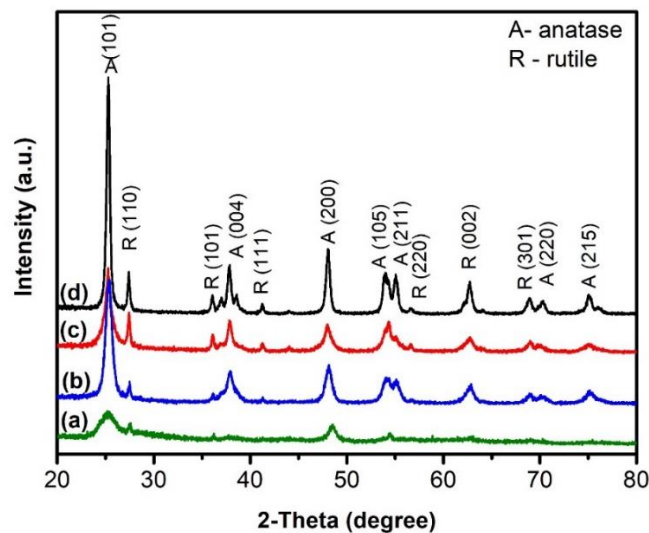


Figure 4: XRD patterns of the photocatalysts, (a) TB - B precursor with modified titanium dioxide (NT), (b) TC - active carbon with modified titanium dioxide (NT), (c) NT - modified TiO<sub>2</sub> P25 and (d) P25 - commercial TiO<sub>2</sub>.

The NT sample profile exhibits peaks in the same positions as those observed for TiO<sub>2</sub> P25 suggesting that the phase composition in these solids was not modified. However, the peaks in NT

are smaller and wider, indicating the formation of structures containing smaller crystals. In the profile of TC a decrease in intensity with wider peaks is also observed, more pronounced for rutile [32]. The diffractogram of TB show broader and less defined peaks, characteristic of the anatase phase. The absence of peaks characteristic of rutile indicates a different structure for the other materials, suggesting that the carbonization of the biomass generating reducing gases, such as CO and H<sub>2</sub>, provided more favorable conditions for stabilization of the anatase phase than for rutile. Another possibility for this is the coating of TiO<sub>2</sub> by charcoal during the carbonization of the mango residue. The TG/DTA curves of the mango residue (B) and the titanium dioxide/mango residue mixture (TB<sub>BC</sub>, BC - before carbonization) are shown in Figures 5 and 6.

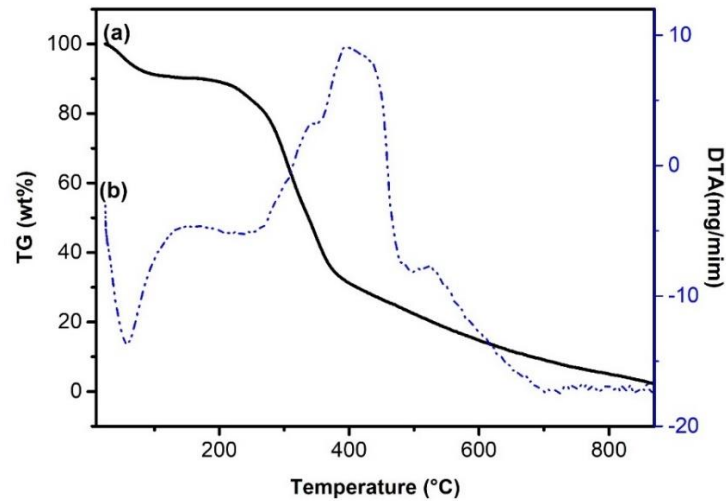


Figure 5: Thermal analysis curves of sample B: (a) TG and (b) DTA.

Three regions of mass loss are observed in the TG curve of precursors B and TB<sub>BC</sub>, with the first one below 100 °C (mass loss of approximately 20%), related to water and volatile losses, and the others between 200 and 500 °C, related to the decomposition of biomass components (loss of mass of approximately 40%). However, the TG curve of sample B shows that there is a mass reverberation at temperatures above 500 °C, remaining to a temperature higher than 800 °C, while in the TG curve of the TB<sub>BC</sub> a temperature stability is observed above 500 °C. The DTA curve of the mango residue (B) shows an exothermic peak with ashoulder at about 340 °C and a maximum at 400 °C. Such thermal effects may correspond to the decomposition of lignocellulosic materials present in the biomass associated with changes in the structure [33].

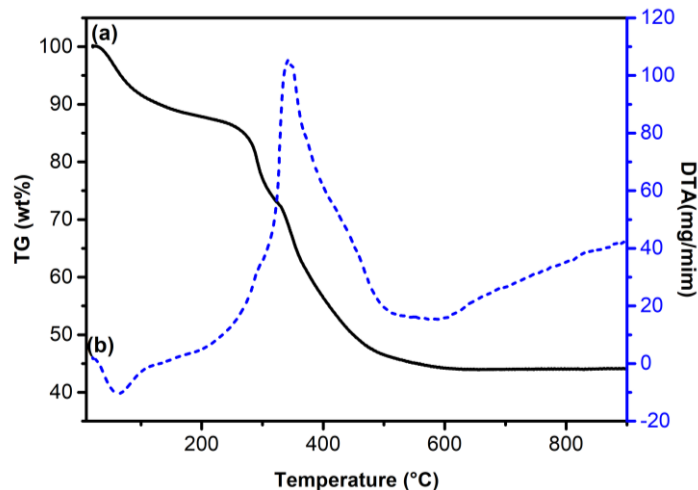


Figure 6: Thermal analysis curves of sample TB<sub>BC</sub>: (a) TG and (b) DTA.

In the DTA curve of  $TB_{BC}$  only one peak is observed with a maximum at approximately 350 °C. This suggests that the decomposition of lignin, cellulose, and hemicellulose present in the mango residue occurs at lower temperatures during the carbonization of B, indicating the influence of titanium dioxide in the process. The absence of other peaks at higher temperatures indicates that there was no phase transformation from anatase to rutile, which occur at temperatures of 600–700 °C [34]. Thus, based on the TG-DTA information, it can be inferred that the carbonization of the precursor  $TB_{BC}$  at a temperature of 500 °C should favour the anatase phase.

Analyzing the curves of the composite titanium dioxide/activated carbon before heat treatment ( $TC_{BC}$ , BC - before carbonization) (Figure 7), a mass loss up to 100 °C is observed, decreasing between 100 and 200 °C, accompanied with an endothermic peak in the DTA curve, which may be associated to the removal of water from the material (mass loss of approximately 20%). Between 200 and 500 °C, the stability of the sample can be observed. From these results, it can be inferred that the  $TiO_2$  content in TC composite remains in 50% (content of the starting material) while in the composite TB the titanium dioxide content is about 62% due the biomass decomposition during the heat treatment temperature (500 °C). Between 500 and 700 °C, a mass variation can be observed in the TG curve, probably due the decomposition of carbon. This is accompanied with two exothermic peaks in the DTA curve at 500 °C, indicating a possible transformation of anatase in rutile, a process that occurs at temperatures higher than 600 °C [35]. From these results, it can be inferred that with thermal treatment of modified titanium dioxide/biomass precursors or modified titanium dioxide/activated carbon at 500 °C in an inert atmosphere, the anatase phase is stabilized with respect to rutile, corroborating with results of X-ray diffraction.

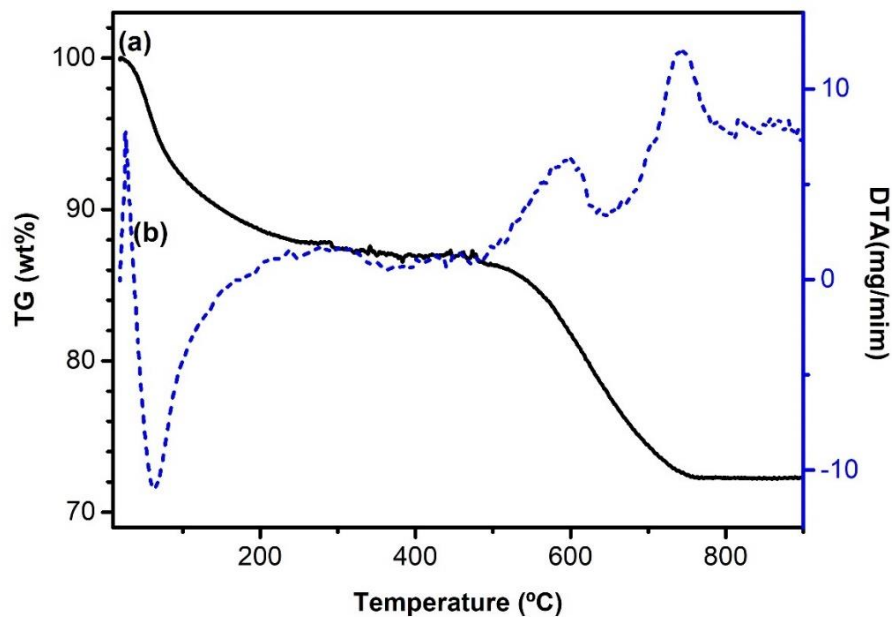


Figure 7: Thermal analysis curves of sample  $TC_{BC}$ : (a) TG and (b) DTA.

The  $N_2$  adsorption/desorption isotherms of the composites follow the type IV, present hysteresis cycles at high pressures ( $P/P_0$ ) (Figure 8), suggesting the presence of mesoporous materials. In the isotherm of the TC sample the occurrence of adsorption is observed at low pressures, suggesting the existence of micropores, which can be attributed to the presence of carbon [36].

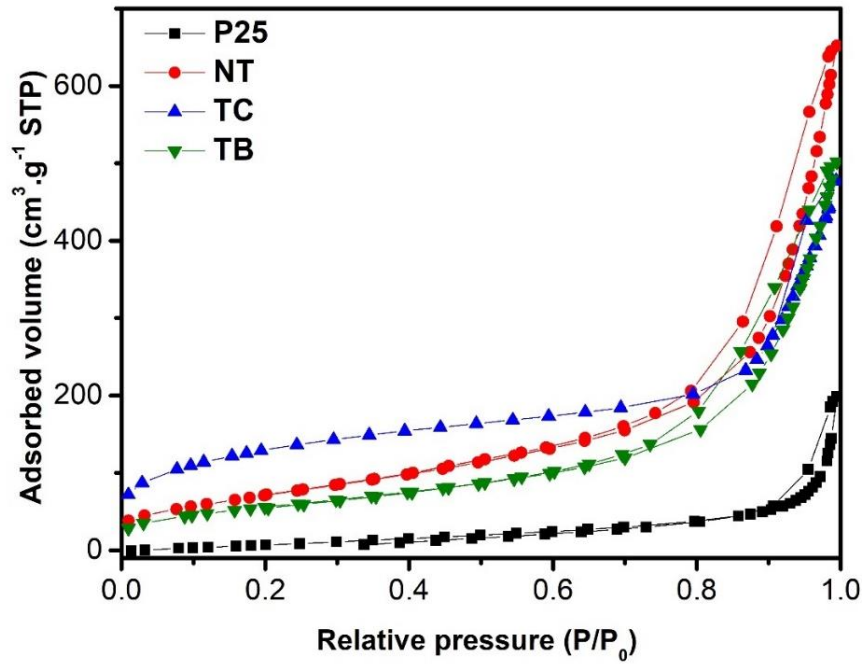


Figure 8.  $N_2$  adsorption/desorption isotherms obtained for the photocatalysts: NT is the modified  $TiO_2$  P25; TC is the active carbon with modified titanium dioxide (NT); TB is the precursor B with modified titanium dioxide (NT) and P25 is commercial  $TiO_2$ .

The calculated specific surface area, mean pore diameter, pore volume and porosity are presented in Table 1. When analyzing these results, it was observed that the alkaline hydrothermal treatment produced a material with a high specific surface area (NT,  $268 \text{ m}^2 \text{ g}^{-1}$ ) when compared to its precursor ( $TiO_2$ ), which may be related to the reduction in size of the crystals observed by XRD [37]. From the value of the mean pore diameter, it can be concluded that all materials have essentially mesoporous structure (2-50 nm). The TB composite showed higher porosity which may be a consequence of the thermal decomposition of the lignocellulosic materials present before heating, resulting in a porous carbonaceous material. The composite TC presented the largest specific surface area, suggesting the positive effect of the association of  $TiO_2$  with activated carbon. The pore size distributions were estimated using the method of Barrett-Joyner-Halenda (BJH) [38], shown in Figure 9. It can be seen a wide distribution of pore sizes in the mesoporous region with average values below 50 nm.

Table 1: Textural features of the samples.

Phtocatalyst	Specific surface area ( $\text{m}^2 \text{ g}^{-1}$ )	Pore diameter (nm)	Pore Volume ( $\text{cm}^3 \text{ g}^{-1}$ )	Porosity (%)
$TiO_2$	70	14.1	0.2	24.4
NT	268	13.5	0.9	55.8
TB	208	14.0	0.7	63.3
TC	471	10.3	0.5	36.7

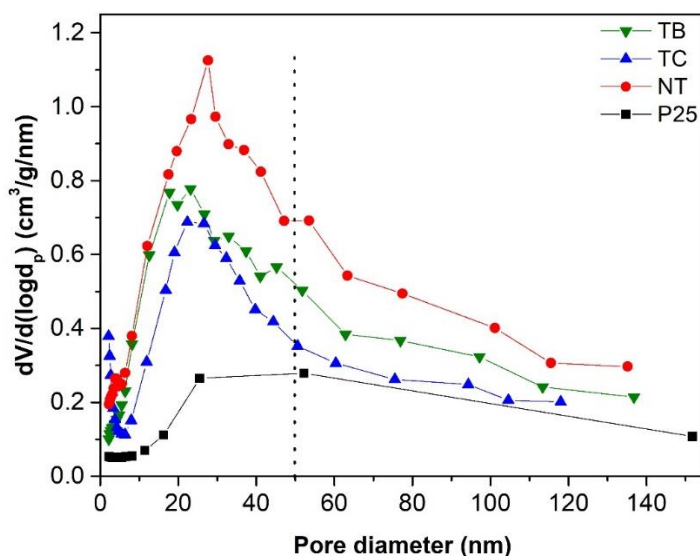


Figure 9: Distribution of pore volume of the materials under study, estimated using the BJH method [38]. NT is the modified  $\text{TiO}_2$  P25; TC is the active carbon with modified titanium dioxide (NT); TB is the B precursor with modified titanium dioxide (NT) and P25 is a commercial  $\text{TiO}_2$  (P25).

Figure 10 shows the SEM images of the mango residue after heat treatment (CB), and active carbon (AC). Thermal treatment of the biomass at  $500^\circ\text{C}$  led to a carbonaceous material with a characteristic morphology of aggregated particles with cavities. Activation using zinc chloride gave rise to the sample (AC), where an increase in the size of cavities was observed, in agreement with the literature [39].

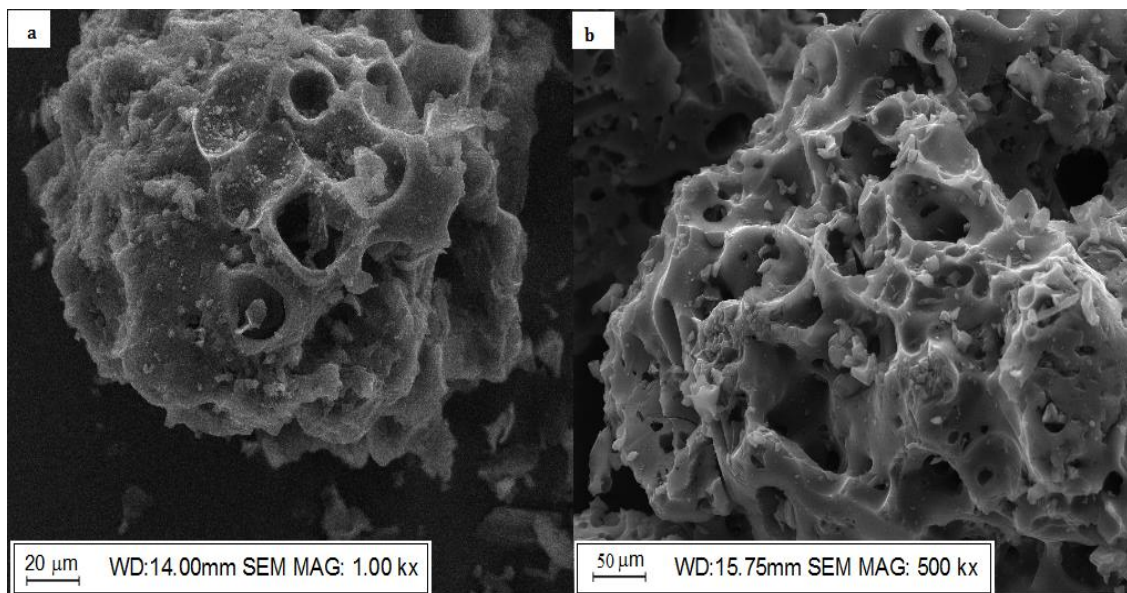


Figure 10: SEM images of the mango residue (a) after carbonization – CB, and of the (b) active carbon – AC.

Figure 11a shows that the NT sample consists of combined crystallites in larger clusters. A possible cause for the formation of agglomerates is the chemical etching and the type of heat treatment that  $\text{TiO}_2$  was submitted for formation of the NT sample. It can be inferred that the NT agglomerates can be distributed on the surface of the carbon and deposited in the opening of the pores of the active carbon [40], which can explain the micro-composition of TC (Figure 11b) and its smaller pore diameter when compared to the other materials. This agrees with X-ray diffraction

data which show that there was no significant change in NT structure after heat treatment of the mixture between NT and active carbon, and with FTIR results that indicated a possible coverage of the carbon by  $\text{TiO}_2$  particles.

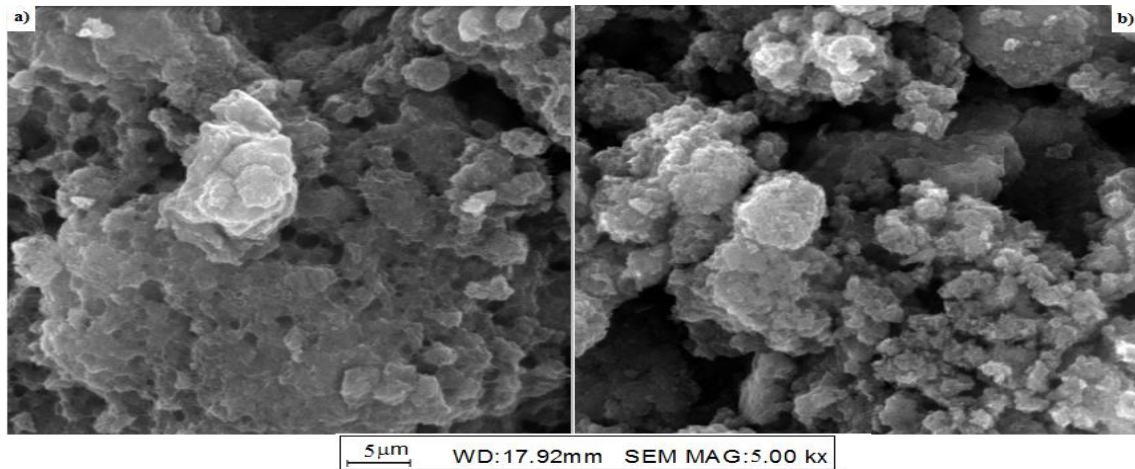


Figure 11: Photomicrography of the (a) modified  $\text{TiO}_2$  - NT and of the (b) composite TC, obtained by combination of  $\text{TiO}_2$  with activated carbon.

The Figure 12 shows the photomicrographs of the composite obtained by association of modified  $\text{TiO}_2$  with the mango residue and submitted to carbonization at  $500^\circ\text{C}$  (TB). It is possible to notice a structure with elongated morphology, evidencing the fibrous nature of the plant materials. It has been observed that titanium dioxide particles are able to partially cover the surface of the carbonaceous material while still maintaining pores, possibly justifying its adsorption in these materials [41].

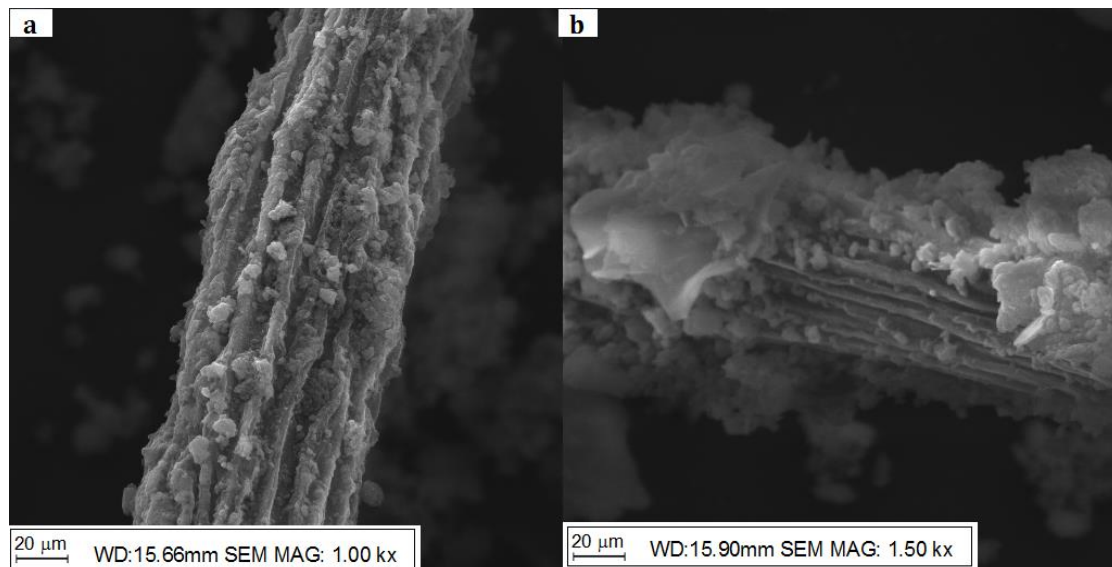


Figure 12: SEM images of the (a) TB composite and (b) precursor B with modified titanium dioxide (NT).

TEM image of the TB composite evidence the formation of irregular spherical roughly dispersed nanoparticles in the carbonaceous material (Figure 13a). The estimated mean size from TEM image is 5.7 nm, according to the histogram (Figure 13b). This value is close to that estimated for crystallite size from X-ray diffractogram (Figure 4), which is 4.1 nm.

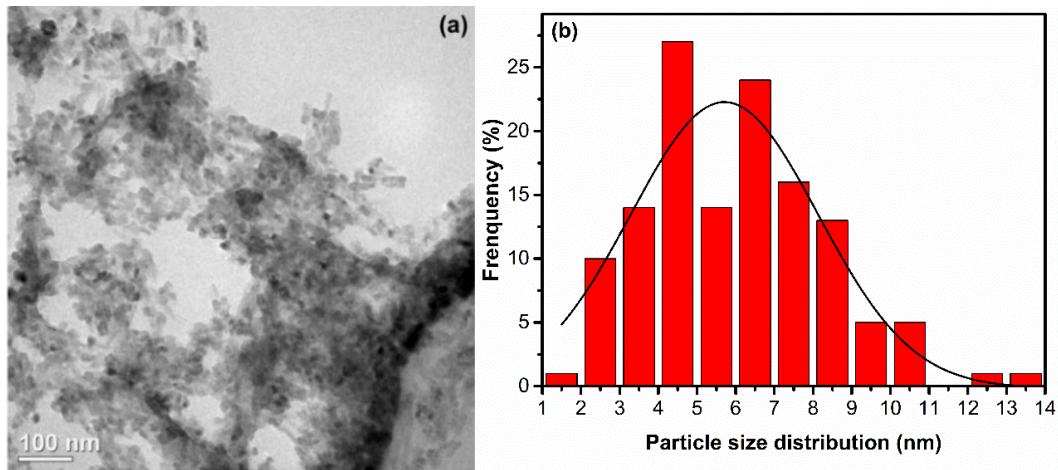


Figure 13: (a) TEM micrograph of the TB composite; (b) Particle size distribution determined from TEM image of TB.

As discussed previously, when compared to other materials obtained, TB presents significant differences in its structural properties (Figure 4). Such differences should be associated with the carbonization process of the biomass/dioxide and titanium blend ( $TB_{BC}$ ). According to the literature, the decomposition of solids with morphological irregularities, as is the case of biomass derivatives, occurs through complex mechanisms and the formation of gaseous products is controlled by nucleation mechanisms involving the formation and growth of nuclei, without restrictions, or through the absorption and fusion thereof. However, in some situations, the diffusion process associated with the production of gases and volatiles may predominate [42]. Comparing the thermal analysis results (TG/DTA) of the precursor of the titanium dioxide/biomass ( $TB_{BC}$ ) composite (Figure 6) and the pure biomass (B) (Figure 5), it is observed that in the presence of titanium dioxide the decomposition of lignin, cellulose, and hemicellulose occurs at lower temperatures, suggesting a kinetic process. In this case, titanium dioxide would act as catalyst in the carbonization of the biomass, altering the intermediate state, which could be responsible for the differences of properties of the obtained composite (TB), when compared to the other materials.

The diffuse reflectance spectra of the studied materials, expressed in terms of the Kubelka-Munk  $F(R)$  function [43] are shown in Figure 14.

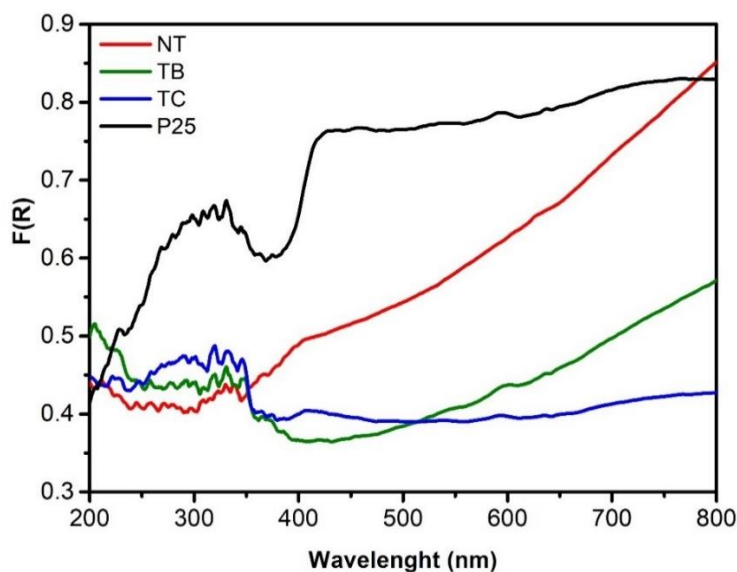


Figure 14: Diffuse reflectance spectra of the photocatalysts: NT is the modified  $TiO_2$  P25; TC is the active carbon with modified titanium dioxide (NT); TB is the precursor B with modified titanium dioxide (NT), and P25 is a commercial  $TiO_2$ .

As can be observed in Figure 14, all the materials with the exception of TiO<sub>2</sub> display similar UV-vis spectra and present an increase in the radiation uptake capacity, mainly in the visible region of the electromagnetic spectrum. This is due to chemical modifications and the subsequent addition of active carbon material (TB and TC) that increases the absorption capability in the visible. As active carbon is active for UV-vis light and changes the transition of TiO<sub>2</sub> [44], it is not possible to estimate the band gap energy of these composite materials.

An inspection in the spectra suggests that the absorption of radiation is only null when  $F(R) \rightarrow 0$ . This suggests the existence of permitted states with energies below the TiO<sub>2</sub> P25 band gap, estimated by the Kubelka-Munk function [43] as being 3.25 eV (381 nm) [45]. TC and TB stands out, presenting an expressive absorption of visible radiation, which extends to the infrared. These results are important because suggest the possibility of using these materials in photocatalytic processes using virtually the entire solar spectrum, one of the limitations for the use of pure titanium dioxide. However, as this property is not determinant in the photocatalytic performance, it is necessary to analyze a set of factors.

Figure 15 show the photocatalytic activity of TiO<sub>2</sub>, NT, TB, and TC, evaluated against the discoloration of crystal violet as a function of the irradiation time. It can be observed that the association between TiO<sub>2</sub> and the carbonaceous materials resulted in a synergism capable of increasing the photocatalytic activity of the oxide, especially using the composite TB, most probably due the higher production rate of hydroxyl radicals and other species active on the surface of these catalysts.

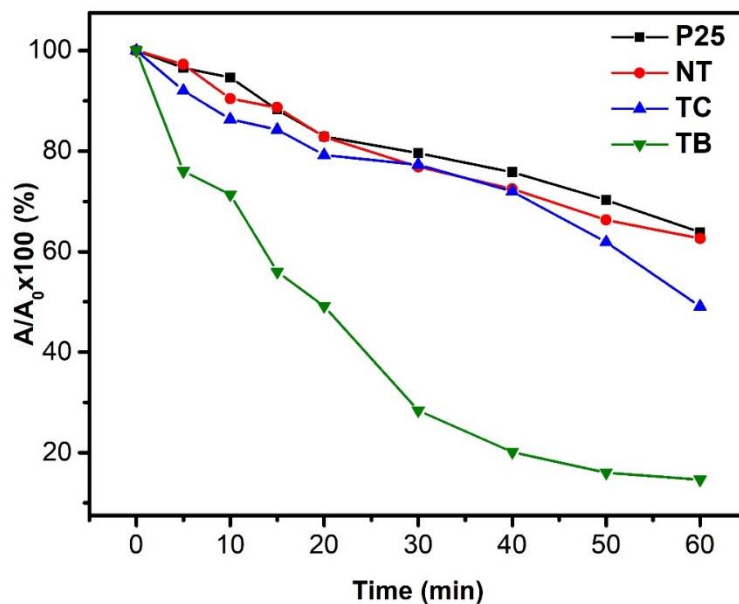


Figure 15: Discoloration of solutions containing crystal violet dye by photocatalysts: P25 is a commercial TiO<sub>2</sub>; NT is the modified TiO<sub>2</sub> P25; TC is the active carbon with modified titanium dioxide (NT) and TB is the precursor B with modified titanium dioxide (NT).

The results shown in Figure 15 show that TB was the most effective photocatalyst in promoting the discoloration of aqueous solutions containing the crystal violet dye. A set of characteristics differentiates TB from the others: morphology with elongated structure (with tube appearance), higher porosity and expressive pore volume (Table 1) and an essentially mesoporous structure, also having a high specific area. In addition, the XRD results suggest that the carbonization process that resulted in this composite provided favourable conditions for the stabilization of the anatase phase, with smaller peaks, suggesting a greater dispersion and/or smaller size, inhibiting the rutile phase, present in both P25 and NT. It is well known that anatase is more photoactive than rutile [46]. However, this does not contribute to better performance since the anatase/rutile combination in P25 delays the recombination of the charge carriers formed at the moment of TiO<sub>2</sub> excitation, which

favours the photocatalytic action of this oxide [46]. On the other hand, the improved textural properties associated with the morphological properties should contribute to a more efficient diffusion of the reactive species involved in the photocatalytic process. This should compensate the recombination of the charge carriers ensuring a differentiated photocatalytic performance for this material, since such parameters are directly associated with the number of active sites.

Another aspect that deserves to be emphasized for these composites is the extension of the absorption of radiation to the visible and the near infrared. It is known that TiO<sub>2</sub> P25 has a limited ability of radiation uptake limited to wavelengths shorter than 400 nm [46]. Although the TB composite exhibits a different absorption spectrum from the other, showing a decline in the photon uptake capability from 400 nm, its photon uptake extends to the near infrared. Despite the fact that TC has practically constant photon uptake capability in the same region covered by TB, TB showed a higher porosity, a preferential anatase phase, and TiO<sub>2</sub> dispersion in the carbonaceous material matrix.

The differentiated performance presented by the composites under study, especially TB, was confirmed by analyzing the efficacy of dye mineralization through dissolved organic carbon (DOC) measurements. A mineralization of more than 60% was achieved with 30 minutes of reaction ( $\text{DOC}_{\text{initial}} = 73 \text{ mg L}^{-1}$ ;  $\text{DOC}_{\text{final}} = 44 \text{ mg L}^{-1}$ ), using the catalysts NT and TC, while TB presented better performance in dye mineralization (99%) after 60 minutes of reaction ( $\text{DOC}_{\text{initial}} = 73 \text{ mg L}^{-1}$ ;  $\text{DOC}_{\text{final}} = 72 \text{ mg L}^{-1}$ ). In other words, the photocatalytic activity of these materials was considerably improved when compared with the results achieved using untreated TiO<sub>2</sub> P25.

#### 4. CONCLUSION

The composites produced by combination of nanoparticles of a commercial titanium dioxide with active carbon or mango residue, resulted in materials with improved photocatalytic properties when compared to the pure catalyst. The composites, especially TB, presented better performances in the photocatalytic degradation of violet crystal, used as model of oxidizable substrate, confirmed by solution discoloration and DOC measurements. A mineralization of more than 60% of the dye was achieved with 30 minutes of reaction time, using the catalysts TB and TC. The TB composite presented better performance for dye mineralization (99%) after 60 minutes of reaction.

#### 5. ACKNOWLEDGMENTS

The authors would like to thank the Applied Chemistry Postgraduate Program (PGQA) of Universidade do Estado da Bahia (UNEB) and Federal University of Uberlândia for the granted infrastructure.

#### 6. REFERENCES

1. El-sayed GO. Removal of methylene blue and crystal violet from aqueous solutions by palm kernel fiber. *Desalination* 2011;272(1):225-232, doi: 10.1016/j.desal.2011.01.025.
2. Wang S, Zhu ZH, Coomes A, Haghseresht, F, Lu GQ. The physical and surface chemical characteristics of activated carbons and the adsorption of methylene blue from wastewater. *J Colloid Interf Sci.* 2005;284(2):440-446, doi: 10.1016/j.jcis.2004.10.050.
3. Ge F, Ye H, Li M, Zhao BX. Efficient removal of cationic dyes from aqueous solution by polymer-modified magnetic nanoparticles. *Chem Eng J.* 2012;198-199:11-17, doi: 10.1016/j.cej.2012.05.074.
4. Dewil R, Mantzavinos D, Poulios I, Rodrigo, MA. New perspectives for advanced oxidation processes. *J Environ Manage.* 2017;195:93-99, doi: 10.1016/j.jenvman.2017.04.010.
5. Pereira PCG, Reimão RV, Pavesi T, Saggiaro, EM, Moreira, JC, Correia, FV. Lethal and sub-lethal evaluation of Indigo Carmine dye and byproducts after TiO<sub>2</sub> photocatalysis in the immune system of *Eisenia andrei* earthworms. *Ecotoxicol Environ Saf.* 2017;43:275-282, doi: 10.1016/j.ecoenv.2017.05.043.
6. Yasmina M, Mourada K, Mohammed HS, Khaoula C. Treatment heterogeneous photocatalysis; factors influencing the photocatalytic degradation by TiO<sub>2</sub>. *Energy Procedia.* 2014;50:559-566, doi: 10.1016/j.egypro.2014.06.068.

7. Arcanjo GS, Mouteer AH, Bellato CR, Silva MM, Dias SHB, da Silva PR. Heterogeneous photocatalysis using TiO<sub>2</sub> modified with hydrotalcite and iron oxide under UV–visible irradiation for color and toxicity reduction in secondary textile mill effluente. *J Environ Manage.* 2018;211:154-163, doi: 10.1016/j.jenvman.2018.01.033.
8. Sui X, Xianhua L, Ting N, Fengsen L, Li G. Carbonaceous-TiO<sub>2</sub> materials: unique morphologies for photocatalytic applications. *J Mater Sci.* 2020;55(7):2725-2740, doi: 10.1007/s10853-019-04224-x.
9. Laciste MT, de Luna MDG, Tolosa NC, Lu MC. Degradation of gaseous formaldehyde via visible light photocatalysis using multi-element doped titania nanoparticles. *Chemosphere.* 2017;182:174-182, doi: 10.1016/j.chemosphere.2017.05.022.
10. Yu A, Wang Q, Wang J, Chang C. Rapid synthesis of colloidal silver triangular nanoprisms and their promotion of TiO<sub>2</sub> photocatalysis on methylene blue under visible light. *Catal Commun.* 2017;90:75-78, doi: 10.1016/j.catcom.2016.11.004.
11. Orha C, Pode R, Manea F, Lazau C, Bandas C. Titanium dioxide-modified activated carbon for advanced drinking water treatment. *Process Saf Environ.* 2017;108:26-33, doi: 10.1016/j.psep.2016.07.013.
12. Begum S, Ahmaruzzaman M. Biogenic synthesis of SnO<sub>2</sub>/activated carbon nanocomposite and its application as photocatalyst in the degradation of naproxen. *Appl Surf Sci.* 2018;449:780-789, doi: 10.1016/j.apsusc.2018.02.069.
13. Leary R, Westwood A. Carbonaceous nanomaterials for the enhancement of TiO<sub>2</sub> photocatalysis. *Carbon.* 2011;49(3):741-772, doi: 10.1016/j.carbon.2010.10.010.
14. Li CJ, Zhao R, Peng M, Hao, L, Gang Y, Dong-sheng X. Study on desulfurization and denitrification by modified activated carbon fibers with visible-light photocatalysis. *Fuel Chem Technol.* 2015;43(12):1516-1522, doi: 10.1016/S1872-5813(16)30004-4.
15. McEvoy JG, Cu W, Zhang Z. Synthesis and characterization of Ag/AgCl-activated carbon composites for enhanced visible light photocatalysis. *Appl Catal B-Environ.* 2014;144:702-712, doi: 10.1016/j.apcatb.2013.07.062.
16. Guodang J, Zhifen L, Chen C, Chang Q, Wang N, Wei W, Tang H. TiO<sub>2</sub> nanoparticles assembled on graphene oxide nanosheets with high photocatalytic activity for removal of pollutants. *Carbon.* 2011;49(8):2693-2701, doi: 10.1016/j.carbon.2011.02.059.
17. He D, Li Y, Wang I, Wang I, Wu J, Yang Y, An Q. Carbon wrapped and doped TiO<sub>2</sub> mesoporous nanostructure with efficient visible-light photocatalysis for NO removal. *Appl Surf Sci.* 2017;391:318-325, doi: 10.1016/j.apsusc.2016.06.186.
18. Foo KY. Effect of microwave regeneration on the textural network, surface chemistry and adsorptive property of the agricultural waste based activated carbons. *Process Saf Environ.* 2018;116:461-467, doi: 10.1016/j.psep.2018.01.022.
19. Onat MD, Vaidya UK, Lungu C. Preparation of industrial sisal fiber waste derived activated carbon by chemical activation and effects of carbonization parameters on surface characteristics. *Ind Crop Prod.* 2017;95:583-590, doi: 10.1016/j.indcrop.2016.11.016.
20. Sousa MSB, Vieira LM, Silva MJM, Lima A. Nutritional characterization and antioxidant compounds in pulp residues of tropical fruits. *Ciênc Agrotec.* 2011;35(3):554-559, doi:10.1590/S1413-70542011000300017.
21. Oliveira NA, Paula DA, Oliveira EB, Saraiva HS, Stringheta PC, Ramos AM. Optimization of pectin extraction from Ubá mango peel through surface response methodology. *Int J Biol Macromol.* 2018;113:395-402, doi: 10.1016/j.ijbiomac.2018.02.154
22. Shoukat S, Iqbal M, SS, Bhatti NH, Noreen S. Mango stone biocomposite preparation and application for crystal violet adsorption: A mechanistic study. *Micropor Mesopor Mat.* 2017;239:180-189, doi: 10.1016/j.micromeso.2016.10.004.
23. Moreno AJP, Moreno MAP, Dorado MP, Agugliano FM. Mango stone properties as biofuel and its potential for reducing CO<sub>2</sub> emissions. *J Clean Prod.* 2018; 190:53-62, doi: 10.1016/j.jclepro.2018.04.147.
24. Chen F, Fang P, Gao Y, Liu Z, Dai Y. Effective removal of high-chroma crystal violet over TiO<sub>2</sub>-based nanosheet by adsorption-photocatalytic degradation. *Chem Eng J.* 2012;204-206:107-113, doi: 10.1016/j.cej.2012.07.030.
25. Ozdemir I, Sahim M, Orhan R, Erdem M. Preparation and characterization of activated carbon from grape stalk by zinc chloride activation. *Fuel process technol.* 2014;125:200-206, doi: 10.1016/j.fuproc.2014.04.002.
26. Tsoncheva T, Mileva A, Tsyntsarski B, Paneva D, Spassova I, Kovacheva D, Velinov N, Georgieva B, Petrov N. Activated carbon from Bulgarian peach stones as a support of catalysts for methanol decomposition. *Biomass Bioenerg.* 2018;109:135-146, doi: 10.1016/j.biombioe.2017.12.022.
27. Kose KO, Piskin B, Aydinol MK. Chemical and structural optimization of ZnCl<sub>2</sub> activated carbons via high temperature CO<sub>2</sub> treatment for EDLC applications. *Int J Hydrog Energy.* 2018;43(40):18607-18616, doi: 10.1016/j.ijhydene.2018.03.222.

28. Sood S, Umar A, Mehta SK, Sinha ASK, Kansal SK. Efficient photocatalytic degradation of brilliant green using Sr-doped TiO<sub>2</sub> nanoparticles. *Ceram Int.* 2015;41(3):3536-3540, doi: 10.1016/j.ceramint.2014.11.010.
29. Ye X, Zheng C, Ma L, Huang X. Microemulsion-assisted hydrothermal preparation and infrared radiation property of TiO<sub>2</sub> nanomaterials with tunable morphologies and crystal form. *Mat Sci Semicon Proc.* 2015;31:295-301, doi: 10.1016/j.mssp.2014.12.019.
30. Lei XF, Xue XX, Yang H, Chen C, Li X, Niu MC, Gao XY, Yang YT. Effect of calcination temperature on the structure and visible-light photocatalytic activities of (N, S and C) co-doped TiO<sub>2</sub> nano-materials. *Appl Surf Sci.* 2015;332:172-180, doi: 10.1016/j.apsusc.2015.01.110.
31. Askari MB, Banizi ZT, Soltani S, Seifi M. Comparison of optical properties and photocatalytic behavior of TiO<sub>2</sub>/MWCNT, CdS/MWCNT and TiO<sub>2</sub>/CdS/MWCNT nanocomposites. *Optik.* 2018;157:230-239, doi: 10.1016/j.ijleo.2017.11.080.
32. Topalov AS, Sojic DV, Molnár-Gábor DA, Abramovic BF, Comor MI. Photocatalytic activity of synthesized nanosized TiO<sub>2</sub> towards the degradation of herbicide mecoprop. *Appl Catal B-Environ.* 2004;54(2):125-133, doi: 10.1016/j.apcatb.2004.06.012.
33. Zhang J, Gao J, Chen Y, Hao X, Jin X. Characterization, preparation, and reaction mechanism of hemp stem based activated carbon. *Results Phys.* 2017;7:1628-1633, doi: 10.1016/j.rinp.2017.04.028.
34. Kordouli E, Dracopoulos V, Valmakis T, Bourikas K, Lucourghiotis A, Kordulis C. Comparative study of phase transition and textural changes upon calcination of two commercial titania samples: A pure anatase and a mixed anatase-rutile. *J Solution Chem.* 2015;232:42-49, doi: 10.1016/j.jssc.2015.08.040.
35. Asilturk M, Sener S. TiO<sub>2</sub>-activated carbon photocatalysts: Preparation, characterization and photocatalytic activities. *Chem Eng J.* 2012;180:354-363, doi: 10.1016/j.cej.2011.11.045.
36. Serafin J, Narkiewicz U, Morawski AM, Wróbel RJ, Michalkiewicz B. Highly microporous activated carbons from biomass for CO<sub>2</sub> capture and effective micropores at different conditions. *J CO<sub>2</sub> Util.* 2017;18:73-79, doi: 10.1016/j.jcou.2017.01.006.
37. Nawi MA, Zain SM. Enhancing the surface properties of the immobilized Degussa P-25 TiO<sub>2</sub> for the efficient photocatalytic removal of methylene blue from aqueous solution. *Appl Surf Sci.* 2012;258(16):6148-6157, doi: 10.1016/j.apsusc.2012.03.024.
38. Barrett EP, Joyner LG, Halenda PP. The determination of pore volume and area distributions in porous substances. I. Computations from Nitrogen Isotherms. *J Am Chem Soc.* 1951;73(1):373-380.
39. Pratumpong P, Toommee S. Utilization of zinc chloride for surface modification of activated carbon derived from *Jatropha curcas* L. for absorbent material. *Data Brief.* 2016;9:970-975, doi: 10.1016/j.dib.2016.11.019.
40. Rengga WDP, Chafidz A, Sudibandriyo M, Naskin M, Abaseed AE. Silver nano-particles deposited on bamboo-based activated carbon for removal of formaldehyde. *J Env Chem Eng.* 2017;5(2):1657-1665, doi: 10.1016/j.jece.2017.02.033.
41. Khalid NA, Majid A, Tahir B, Niaz NA, Khalid S. Carbonaceous-TiO<sub>2</sub> nanomaterials for photocatalytic degradation of pollutants: A review. *Ceram Int.* 2017;43(17):14552-14571, doi: 10.1016/j.ceramint.2017.08.143.
42. Khawam A, Flanagan DR. Solid-state kinetic models: basics and mathematical fundamentals. *J Phys Chem B.* 2006;110(35):17315-17328, doi: 10.1021/jp062746a.
43. Patterson EM, Sheldon CE, Stockton BH. Kubelka-Munk optical properties of a barium sulfate white reflectance standard. *Appl Opt.* 1977;16(3):729-732.
44. Liu X, Wang X, Xing X, Li W, Yang J. Visible light photocatalytic activities of carbon nanotube/titanic acid nanotubes derived-TiO<sub>2</sub> composites for the degradation of methylene blue. *Adv Powder Tech.* 2015;26(1):8-13, doi: 10.1016/j.apt.2014.11.003.
45. Hoffmann MR, Martin ST, Choi W, Bahnemann DW. Environmental applications of semiconductor photocatalysis. *Chem Rev* 1995;95(1):69-96, doi: 10.1021/cr00033a004.
46. Bellardita M, Paola AD, Megna B, Palmisano L. Determination of the crystallinity of TiO<sub>2</sub> photocatalysts. *J Photoch Photobio A.* 2018;367:312-320, doi: 10.1016/j.jphotochem.2018.08.042.